Post-print of: Panuszko A., Bruździak P., Śmiechowski M., Stasiulewicz M., Stefaniak J., Stangret J.: DMSO hydration redefined: Unraveling the hydrophobic hydration of solutes with a mixed hydrophilic–hydrophobic characteristic. JOURNAL OF MOLECULAR LIQUIDS. Vol. 294 (2019). DOI: 10.1016/j.molliq.2019.111661

DMSO hydration redefined: unraveling the hydrophobic hydration of solutes with a mixed hydrophilic–hydrophobic characteristic

A. Panuszko, P. Bruździak, M. Śmiechowski, M. Stasiulewicz, J. Stefaniak, and J. Stangret*

Department of Physical Chemistry, Gdańsk University of Technology, Narutowicza 11-12, 80-233 Gdańsk, Poland

Abstract

Hydrophobic hydration of solutes with a mixed hydrophilic–hydrophobic characteristics is still poorly understood. This is because both experimental and theoretical methods find it difficult to see the ice-like water structure around the nonpolar solute groups, unlike hydrogen bonds with the hydrophilic groups. In order to unravel this problem, we have investigated DMSO hydration by means of infrared spectroscopy and theoretical methods, namely DFT, ONIOM calculations and AIMD simulations, which allowed us to redefine its hydration. In dilute DMSO solutions the clathrate-like water is formed around the DMSO molecule, supported by interactions of water molecules with the methyl hydrogens (the blue-shifted hydrogen bonds). The cage is constructed by water molecules that form hydrogen bonds of the comparable energy and length with the SO group and between water molecules. When the construction of the cage is completed, DMSO molecule partially regains its rotational freedom inside. Strong hydrogen bonds within the frame

*janusz.stangret@pg.edu.pl

are masked by the relatively small population of weakened hydrogen bonds of water molecules in the vicinity of the SO group, due to the improper fit to the bulk water of water molecules hydrogen bonded to the oxygen atom of DMSO. We also propose a new explanation of the highly non-ideal mixing behavior of aqueous DMSO solutions at the eutectic point, as the positive excess entropy of the equimolar amounts of molecular complexes distinguished in the system.

Keywords: Water structure, Hydrophobic hydration, DMSO-water complexes, FTIR spectroscopy, DFT calculations, AIMD simulations

1. Introduction

"Water is an active matrix of life for cell and molecular biology" [1]. In this sense, the role of water relies on its diverse structural and dynamic characteristics in such systems. One of the very important specific structural forms which water adopts near non-polar surfaces of biomolecules is known as the hydrophobic hydration which contributes to many chemical and biochemical processes, such as protein folding, protein–protein, and protein–co-solute or self–assembly of lipid membranes [2, 3, 4, 5, 6, 7, 8, 9, 10]. However, since the formulation of the "iceberg formation" hypothesis by Frank and Evans [11], opinions on the water structure near the non-polar fragments of solutes have been inconsistent (see for example ref. [12] for a review). Recently, their model has been confirmed by Grdadolnik *et al.* [13] by means of the high-pressure infrared spectroscopy for small purely hydrophobic solutes (methane, ethane, krypton, and xenon). The strengthened water structure in such cases is similar to the one of ice or solid clathrates. Other direct

experimental evidence has also been demonstrated [14, 15], however, studies of soluble solutes with both hydrophilic and hydrophobic moieties elude any simple explanation of their complex hydration [16, 17]. Dimethyl sulfoxide (DMSO) is a simple molecule which can serve as a model for studying such a type of mixed hydration.

DMSO is an aprotic solvent and its aqueous solutions have many interesting physicochemical and biological properties. DMSO is miscible with water in all proportions [18]. Dielectric spectroscopy studies of liquid DMSO have proven the existence of its dimers and longer forms ("polymers") with anti-parallel ordering of molecular dipoles [19, 20]. Numerous studies have revealed uncommon physicochemical properties of DMSO–water system, manifested by strong deviations of their thermodynamic properties from ideality [21]. Many reports indicate that water–DMSO hydrogen bonds are stronger than those between water molecules [19, 20, 22]. As a result of these interactions, molecular complexes of water and DMSO are relatively stable, regardless of composition [23]. It is assumed that the unusual features of DMSO solutions are due to the various species water–DMSO complexes [24, 25]. These clusters at various DMSO concentrations have been extensively studied both experimentally [20, 21, 26, 24, 25, 27] and theoretically [23, 24, 28, 29, 30, 31]. Those which consist of $3DMSO{\cdot}1H_2O$, $2DMSO{\cdot}1H_2O$, and $1DMSO{\cdot}1H_2O$ have been found at mole fractions of water (x_w) lower than 0.5 [21, 23, 25]. The strongest deviations from ideality and the strongest hydrogen bonds occur at x_w between 0.6 and 0.7 [26, 32, 17]. The presence of stable $1DMSO{\cdot}2H_2O$ aggregate has been observed in this range [20, 26]. It is also the eutectic composition with freezing temperature of ca. –70 °C

[33], while freezing points of water and DMSO are 0 °C and 18.6 °C, respectively. But according to the hypothesis of Kirchner and Reiher [31], many energetically similar but structurally different complexes exist in the DMSO–water mixture near the eutectic point. They proposed the mechanism of the clusters' influence on the non–ideal mixing behavior of these systems.

There is no general agreement on the influence of DMSO on water structure. The results of experimental studies [34, 35, 36, 37] and computer simulations [28, 35, 38, 39] indicate that water structure is enhanced in dilute DMSO aqueous solutions. On the other hand, some experimental studies [20, 40, 41] lead to the conclusion that water structure is weakened at a low concentration of DMSO. The experimental techniques, including IR spectroscopy and MD simulations demonstrate that DMSO acts as a "structure breaker" at high concentrations of DMSO [28, 37].

In this paper, we examine the hydration of dimethyl sulfoxide (DMSO) in the whole mole fraction range by means of the FT-IR spectroscopy and computational methods. We demonstrate the existence of the "ice-like" water cage around DMSO molecules in diluted solutions, which enables partial rotational freedom of the guest molecule inside the water cage. We propose also a novel explanation of the strong deviation from ideality of aqueous solutions of DMSO at concentration corresponding to the eutectic point of the system.

2. Materials and methods

2.1. Chemicals and solutions

Dimethyl sulfoxide (99.9%, Alfa Aesar) and D_2O (isotopic purity 99.9%, Aldrich) were used as supplied to prepare solutions without purification. Water used to prepare these solution was deionized (<0.01 $S \cdot cm^{-1}$). All solution have been prepared by weight and their densities were determined with Anton Paar DMA 5000 densitometer at $25.000 \pm 0.001\,^{o}C$. The solution preparation procedure for FTIR measurements of HDO spectra has been described in Supporting Material in ref. [42].

2.2. FTIR spectroscopy

All FTIR spectra of aqueous solutions of DMSO were recorded on the IFS 66 Bruker spectrometer. The spectrometer was purged with dry nitrogen during the measurement. A liquid transmission cell (model A145, Bruker Optics) was equipped with two CaF_2 windows separated by teflon spacers. For H_2O transmission spectra of DMSO-water mixtures for high concentration of DMSO (in the range of $\nu_{S=O}$ vibration), 512 independent scans were taken with resolution of $2\,cm^{-1}$. The path length was equal to 0.0053 mm, as determined interferometrically. In the case of HDO spectra, in the range of ν_{OD} vibration 256 independent scans were taken with the resolution of $4\,cm^{-1}$. The path length was equal to 0.0306 mm, as determined interferometrically. The same path length was used also in the case of spectra for $DMSO \cdot H_2O$ mixtures for very low DMSO concentration, in the range of the $\nu_{S=O}$ vibration band. The temperature was kept at $25.0 \pm 0.1\,^{o}C$ and monitored using thermocouples placed in the sample cell.

The spectra have been analyzed using the following commercial software: GRAMS/32 (Galactic Industries Corp.) and RAZOR (Spectrum Square Associates, Inc.) run under GRAMS/32.

2.3. Analysis of vibrational spectra

The difference spectra method was applied to extract the DMSO-affected HDO spectrum on the basis of spectra series measured for different molalities of aqueous solutions. An assumption was made that the water in solution can be divided into two additive contributions: the bulk water (pure water) and the "solute-affected" water (modified by interactions with the solute). The method of analysis of the spectral data towards extraction of solute-affected water spectrum was described in details in refs. [43, 44, 45] and some of the most basic information are included in the Supplementary Material. The difference spectra method was also applied to the DMSO spectra in the range of the ν(S=O) vibrations to separate specific states of the S=O oscillators.

The factor analysis, in the version written by Malinowski [46], was performed using the commercial computer program Factor Analysis Toolbox for MATLAB (Applied Chemometrics Inc., Sharon). The spectral data were assembled into matrices of absorbances at given wavenumbers and concentrations of DMSO–water mixtures. The main application of this method was window factor analysis (WFA) [47], which involves the extraction of the concentration profiles of the individual chemical species contributing to the spectral data (i.e. factors). The correct number of these factors was obtained by using the basic principal factor analysis algorithm (PFA).

2.4. Theoretical calculations

2.4.1. DFT and ONIOM calculations

All calculations were performed with the GAUSSIAN 09 v.D1 software [48] available at the Academic Computer Center in Gdansk (TASK). The program Avogadro was used to prepare of input data and for visualization of computed results. The analysis of resulting wavefunction files, involving the reduced density gradient (RDG) method [49], was performed with the Multiwfn software v.3.3.9 [50]. The RDG method allowed to visualize weak interaction sites (hydrogen bonds, van der Waals interactions, steric clashes) in molecular complexes and to classify them according to their strengths. All RDG-related figures are presented in the stereo view for better clarity. The D3 version of Grimme's empirical dispersion correction, including the Becke–Johnson damping (GD3-BJ), was applied [51].

Structures of medium-sized complexes: 1DMSO·nH_2O (where n = 1÷15), 3DMSO·2H_2O, and 3DMSO were optimized using the density functional theory (DFT) level with the B3LYP hybrid exchange-correlation functional [52, 53] and 6-311++G(d,p) basis set [54]. The conductor-like polarizable continuum model (CPCM) of the self-consistent reaction field theory (SCRF) was used to simulate the solvent environment [55, 56]. In the case of three different types of the considered complexes: 1DMSO·nH_2O, 3DMSO·2H_2O, and 3DMSO, the following solvents were used: water, solvent mixture of DMSO:water with a mixing ratio of 3:2, and DMSO, respectively.

For more complex structures of one DMSO molecule with up to 100 hydration water molecules the ONIOM approach was applied [57]. 5 to 90 water molecules were added to the DMSO molecule with a step of 5 molecules. Ad-

ditional complexes with 2 to 4 molecules were prepared, however, a more reliable results for such complexes were obtained with the method presented in previous paragraph thanks to the larger basis set and the use of the CPCM solvent model. Initial complexes were optimized with a simple MMFF94a force field [58, 59]. Next, the central DMSO molecule was selected for the high level of ONIOM calculations – B3LYP/aug-cc-pVQZ, and all water molecules for the low level – B3LYP/cc-pVDZ, all performed *in vacuo*. Such a selection of basis sets allowed to obtain satisfactory structures within a reasonable calculation time.

Three different water clusters have been used to obtain the reference parameters for hydrogen bonds energies between solvent molecules: 1) a triangle prism, or nano-drop of 6 molecules for medium-sized complexes, 2) an unstructured complex of 100 molecules for ONIOM-based calculations.

2.4.2. AIMD simulations

AIMD simulations [60] were performed using the DFT-based QUICKSTEP electronic structure module [61] of the CP2K 6.0 computational suite [62, 63]. We applied the BLYP functional [52, 64] together with the DFT-D3 empirical dispersion correction [65]. The cutoff for the latter was set to 16 Å. QUICKSTEP defines a mixed Gaussian type orbitals plus plane waves (GPW) basis set scheme [66], and we used a TZV2P basis set for atomic orbitals and a 500 Ry cutoff for the plane wave expansion of the electron density. Only valence electrons were treated explicitly, while the core electrons were represented by GTH pseudo potentials [67].

The two studied systems consisted of bulk H_2O (80 molecules) and a $DMSO(H_2O)_{80}$ solution, contained in cubic supercells with applied periodic

boundary conditions. In order to compare directly to the FTIR HDO/H_2O spectra, all water hydrogen atoms were given the mass of deuterium, i.e., we effectively simulate D_2O. Initial volumes of the systems were chosen to reflect the experimental density of heavy water [68] combined the apparent molar volume of the DMSO solution [69]. While the experimental data were measured at 298 K, we apply a slight temperature overscaling, typical for AIMD simulations neglecting nuclear quantum effects, in order to recover the proper diffusional behavior of individual molecules in our systems and to avoid the 'glassy dynamics' regime [70]. The extent of this scaling is slight for D_2O ($T = 323.15$ K)[71].

Both systems were first equilibrated for at least 20 ps with a time step of 0.5 fs in the NVT ensemble using massive Nosé-Hoover chain thermostatting [72]. After the equilibration period, 20 initial conditions were sampled every 3 ps from a further NVT simulation to initialize microcanonical (NVE) trajectories of 20 ps length each. During these runs the centers of maximally localized Wannier functions (MLWFs) [73] were computed every 2 fs. All analyzed observables were averaged over the NVE trajectories yielding proper canonical averages.

Molecular dipole moments were obtained classically by summing over positive nuclei and negative MLWF centers. The IR spectra were calculated as Fourier transforms of time correlation functions of dipole moment finite differences [74, 75] using various recently introduced dipolar decomposition schemes for solute–solvent systems, see refs. [75, 76] for details. The spectral resolution was set to 1 cm^{-1} by setting the upper limit of the correlation time to ~ 16.66 ps and the final spectra were smoothed by passing through

a 20 cm^{-1} Gaussian filter. Numerical Kramers–Krönig transform was used to remove the refractive index contributions to the IR spectra [75] using the experimental refractive index of D_2O, $n_D = 1.328$ [77].

3. Results and discussion

3.1. FTIR spectra of HDO in DMSO-water mixtures

HDO spectra in the range of the ν(OD) vibrations are shown for all compositions of the DMSO–water mixture in Fig. 1a. It is clear that the spectral series exhibits two isosbestic points: the first one at ca. 2600 cm^{-1} corresponding to the spectra from pure water to $x_w = 0.83 \pm 0.07$, and the second one at ca. 2530 cm^{-1} corresponding to spectra from the smallest dilutions of water in DMSO to $x_w = 0.41 \pm 0.01$.

The main parameters of the HDO spectra as a function of x_w are presented in Fig. 1b (and also in the Supplementary Material, see Fig. S2). Particularly noteworthy is the dependence for ν(OD) band position at maximum and at the center of gravity of the band. The first one serves as a measure of the most probable energy of hydrogen bonds of water (as well as the most probable O···O distance), and the latter as a measure of the average energy of hydrogen bonds (as well as the average O···O distance).

——Figure 1——

In simple terms, DMSO dissolved in water in larger quantities should be classified as a water "structure-breaking" solute. Only in the range of high dilutions, above ca. 0.8 mole fraction of water, DMSO can be considered as a "structure-making" agent. This may be inferred from the position of the center of gravity of the ν(OD) band, which is red-shifted relative to the

pure water, Fig. 1b. This conclusion is in agreement with other IR studies [37]. The DMSO–water interaction is stronger than water–water interaction: the energy of vaporization of water from DMSO (infinitely diluted solution of water) equals to 46.87 kJ·mol^{-1} vs. 41.53 kJ·mol^{-1}, which corresponds to the energy of vaporization of pure water [78]. The results of the DFT calculations confirm this result: interactions of water molecules with the oxygen atom of S=O group are stronger than those between water molecules in the pure water (see Fig. S7 in the Supplementary Material). This is also in agreement with the structural data obtained from the AIMD simulations: the O$\cdots$O distance in pure D_2O is 0.02 Å longer than the $O_{DMSO}\cdots O_{D_2O}$ distance; see Fig. S10 and Table S2 in the Supplementary Material. On the other hand, this is a typical situation for the aprotic solvent–water systems for which solvent–water interactions are stronger than water–water interactions [78, 79]. Further explanation can be found in the Supplementary Material (section S1.3).

3.1.1. DMSO-affected HDO spectra at high water concentration

Fig. 2a shows DMSO-affected HDO spectra for high water content in the mixtures, along with the affected spectrum obtained for solution of DMSO infinitely diluted in water, the bulk HDO and the dependence of the affected number (i.e. number of moles of water molecules affected by one mole of DMSO, N), on the water mole fraction (see the inset). It should be noted that this parameter generally does not correspond to a hydration number in strict sense, it rather shows the number of solvent molecules statistically influenced by a solute. Because of lability of the hydration sphere for the most of solutes, only a few water molecules appear to be influenced in their proximity, the rest

resembling bulk water. This way, the solute-affected spectrum represents the water status in the "concentrated form". As it can be seen in Fig. 2a, DMSO-affected ν(OD) band positions are blue-shifted relative to the bulk water and, on visual inspection, do not show complex structure. The most interesting seems to be the variability of the derivatives $(d\varepsilon(\nu)/dm)_{m=m_i}$ obtained for the molalities of DMSO (m_i) corresponding to the water mole fractions shown in the inset in Fig. 2a. The derivative corresponding to the infinite dilution of DMSO in water ($m_i = 0$) is characterized by two occurrences of the maximum increase of absorption: (1) at 2538 cm^{-1}, which belongs to water molecules with weaker hydrogen bonds than in the bulk water, and (2) at 2438 cm^{-1}, which corresponds to the strong hydrogen bands of water, as in the case of ice [13]. The last component quickly loses its intensity with the increase of DMSO content in solution and virtually disappears at $x_w \simeq 0.85$, while the first component remains at its place.

——Figure 2——

For further discussion of the observed spectral effects, we will use the transformation of the DMSO-affected water band-shape to the interatomic oxygen–oxygen (O···O) distance distribution function between water molecules, $P(R_{OO})$, as described in ref. [45]. The "O" symbol can also denote the oxygen atom of the S=O group, when the oxygen atom of this group is hydrogen bonded with water molecules. Fig. 2b shows the differences in interatomic O···O distance distribution functions, $\Delta P(R_{OO})$, between DMSO-affected water (for water at infinite dilution or for water at $x_w \simeq 0.85$) and the bulk water. These differences qualitatively resemble the features of the evolution of the derivative $(d\varepsilon(\nu)/dm)_{m=m_i}$ in Fig. 2a. However, the difference deter-

mined for DMSO-affected water at $x_w \simeq 0.85$, $\Delta P(R_{OO})_{\mathrm{x=0.85}}$ (Fig. 2b), still shows an increase of the population of water at short O···O distances, corresponding to the ice-like structure, but this population is much smaller than for the solution at infinite dilution.

As the water concentration increases ($x_w > 0.85$), the water cage around DMSO molecule develops, thus increasing the population of strong hydrogen bonds between the water molecules surrounding the methyl groups. This increase is illustrated by the derivative $(d\varepsilon(\nu)/dm)_{m=m_i}$ (Fig. 2a) and the $\Delta\Delta P(R_{OO})$ function (Fig. 2b). The structural and energetic state of the DMSO hydration water at the infinitely diluted solution is characterized by the $\Delta P(R_{OO})_{\mathrm{x=1}}$ function in Fig. 2b. Accordingly, it should be assumed that for $x_w > 0.85$ strong hydrogen bonds are formed by water molecules both (1) interacting with the S=O group of DMSO, as well as (2) participating in the hydrogen bond network around methyl groups. These two groups of strongly bound water molecules were confirmed by DFT calculation (see Fig.S7 in Supplementary Material). As it can be seen, in terms of the O···O distance both types of hydrogen bonds are poorly distinguishable for small hydration complexes. However, a tendency can also be observed for hydrogen bonds with the S=O group to become weaker as the water cage develops. Only a small population of the water molecules in the hydration shell can be regarded as weakened, as evidenced by the presence of a maximum at ca. 2.90 Å in the $\Delta P(R_{OO})_{\mathrm{x=1}}$ function. This population is also visible on the corresponding difference obtained from AIMD simulation (Fig. 3b) and reflects the water–water hydrogen bonds around the DMSO oxygen atom (explanation in section 3.1.2).

3.1.2. Confrontation of experimental results with those obtained from AIMD simulations

It is most instructive to confront the experimental HDO spectra in the ν(OD) range with the computational IR spectra of D_2O obtained from AIMD simulations (see section S4.4 in the Supplementary Material for implementation details). The representative distance-dependent IR spectra that selectively capture the absorption of the solute–water complex up to a specified cutoff radius R_c are shown in Fig. 3a. Simultaneously, the hydrogen bond definitions (see section S4.1 in the Supplementary Material) have been used to obtain interatomic oxygen–oxygen distance distribution functions corresponding to the experimental ones.

——Figure 3——

Compared to the experimental liquid D_2O spectrum [80], the respective IR spectrum computed on the basis of AIMD simulations is red-shifted by $\sim$ 90 cm^{-1}. This magnitude of the red shift is typical of the liquid water simulations using the generalized gradient approximation (GGA)-based functionals [76, 81] and in explicit inclusion of nuclear quantum effects (NQE) is required to obtain a better agreement with experiment [82, 83]. However, even in the absence of NQE the band shifts obtained from the distance-dependent spectra can be meaningfully compared to experiment [76, 84].

We first focus on the spectrum of DMSO molecule extracted from the aqueous solution. As demonstrated previously, such spectra record important information about the hydration shell due to the dipole moment induced by the solvent's local electric field and the appearance of the thus allowed vibrational transitions in the IR spectrum [76, 84]. In the case of DMSO,

the band position at maximum is blue-shifted by 44 cm^{-1}. Coincidentally, this is in perfect agreement with the experimental ν(OD) band shift for HDO infinitely diluted in DMSO (section S1.3 in Supplementary Material). Since for other hitherto studied solutes similar effects can be observed (i.e., the band shift in the distance-dependent IR spectra is the most pronounced at the vanishing cutoff radius), we hypothesize now that the solute molecule extracted from the solution encodes in a unique way the energetic state of the water molecules at their most perturbed state in the solution, such as at the limit of the infinite dilution in the given solvent.

With the increasing cutoff radius, the distance-dependent IR spectra undergo major changes in the position and the intensity of the water stretching band [76]. These changes can be monitored selectively at a chosen probe wave number, here taken as the position at maximum of the band at $R_c \to 0$, $\nu^\circ = 2461$ cm^{-1}; see inset in Fig. 3a. With increasing R_c, the intensity of the ν(OD) band also increases and reaches a local maximum at $R_c = 3.8$ Å. This particular cutoff radius is then selected as the most representative of the DMSO–water complex. The ν(OD) band position at maximum at this R_c is blue-shifted by 16 cm^{-1}, in excellent agreement with the experimentally observed shift by 11 cm^{-1} (2519 $cm^{-1}{}_{(\nu^\circ_{\mathrm{DMSO}})}$ – 2508 $cm^{-1}{}_{(\nu^\circ_{\mathrm{bulk}})}$, values for the infinite dilution solution, see Table S1 in Supplementary Material). Simultaneously, we can obtain the normalization factor for the distance-dependent IR spectra and thus determine the fractional number of water molecules in the considered solute-centered sphere. It is found to be equal to 3.2 ± 0.6 (the uncertainty is based on the uncertainty of the R_c value, ±0.1 Å), also in perfect correspondence with the experimental affected number $N = 2.8$

(value for the infinite dilution solution, see inset in Fig. 2a and Table S1 in Supplementary Material). Thus, our distance-dependent IR spectra firmly support the results of the analysis of the experimental data with the affected spectra method.

To further explore the parallel character of experimental and computational IR spectra, we again turn to the interatomic oxygen–oxygen (O$\cdots$O) distance distributions; see Fig. 3b. We monitor the changes in the geometry of the hydrogen bond network with respect to bulk water by applying the distance distribution differences, $\Delta P(R_{OO})$, by analogy to the analysis of experimental spectra (section 3.1.1). By selectively computing $P(R_{OO})$ functions around specific sites of DMSO, the local state of the hydrogen bond network can be revealed. As seen in Fig. 3b, the distance distributions around DMSO oxygen undergo much more pronounced changes than around the methyl groups. Interestingly, the $O_{DMSO}\cdots O_{water}$ hydrogen bonds show a completely different trend that the water–water hydrogen bonds in which water molecules located in the first hydration shell around DMSO oxygen are involved. While the former are found to be strengthened with respect to the bulk water, in accordance with the previously discussed DFT studies of static aqueous clusters (see Fig. S7 in the Supplementary Material), the latter are weakened, possibly because the water molecules involved in short hydrogen bonds with O_{DMSO} have trouble with incorporating into the extended hydrogen bond network. The weakening of hydrogen bonds of water is also illustrated in the appropriate distance distribution difference obtained from the spectral data Fig. 2b. On the other hand, the water–water hydrogen bonds around the hydrophobic groups show only a slight reduction of weak

elongated hydrogen bonds with the corresponding appearance of medium- and short-length bonds, but this behavior is qualitatively in agreement with the discussion of the experimental results presented above. We note that similar enhancement of the hydrogen bond network around the hydrophobic groups of TMAO has been recently found [85].

3.2. FTIR spectra of DMSO in aqueous solutions

3.2.1. Spectra in the range of ν(S=O) vibrations

The results of FTIR studies of DMSO–water mixtures in the entire composition range for the ν(S=O) band are summarized in Fig. 5. Spectra shown in Fig. 5a correspond to the ν(S=O) vibrations in the 975–1150 cm^{-1} range, while the band at ca. 950 cm^{-1} is due to the rocking vibrations of DMSO methyl groups [86]. The assignment of the two low-wavenumber components of the complex band of the ν(S=O) vibrations solely to the methyl rocking modes, as in refs [25, 87, 88], is not justified in view of the most recent reassignment which concludes that the CH_3 rocking modes are actually tightly coupled with the ν(S=O) band [89].

——Figure 5——

As it can be seen in Fig. 5a, the addition of water to DMSO significantly changes the shape and the position of the ν(S=O) band. Generally, the increase of water mole fraction (x_w) results in the decrease of the high-wavenumber component of the SO band (band fitting procedure indicates that this component disappears at $x_w \simeq 0.6$), while the other two components are red-shifted and their total intensity increases. It is difficult to identify their individual behavior, because most probably these component bands exchange positions at $x_w \simeq 0.4$. The overall spectral changes observed

in the case of these two component bands are typical for the proton acceptor group forming a hydrogen bond, in this case with water molecules. Our AIMD simulations show that (at $x_w \simeq 0.988$) on average 2.5 hydrogen bonds are formed between the DMSO oxygen and the water molecules; see Figs. S8 and S9 in the Supplementary Material. It is worth noting that the band at ca. $950\,cm^{-1}$ exhibits a similar behavior. When the mole fraction of water exceeds ca. 0.98 (water to DMSO molar ratio higher than 50) unexpected spectral changes take place: the intensity of the SO band decreases, accompanied with a small blue-shift, but at the same time its high-wavenumber part, which corresponds to the vibration of the SO group of DMSO in the gas phase [87, 90] increases. This absorption band is broad and flat and its intensity increases with the DMSO dilution. In another work [89] this band was not analyzed and was probably treated as a background.

3.2.2. Molecular complexes of water and DMSO – analysis of the ν(S=O) vibration bands

It can be expected that fragments of DMSO linear clusters may also exist in aqueous solutions, resulting mainly from dipole–dipole interactions and the CH···O=S blue-shifted hydrogen bonds. [91]. To check this hypothesis we have removed the contribution of the liquid DMSO spectrum from the measured spectra of DMSO–water mixtures shown in Fig.5a. The results are shown in Fig. 5d, which presents the corresponding dependence of the relative contribution of DMSO not forming hydrogen bonds with water. Residual spectra after this treatment (shown in Fig.S1 in the Supplementary Material) should correspond to the spectra of DMSO forming hydrogen bonds with water. Their position vs. x_w is shown in Fig. 5b. A straight line connecting

the extreme values of the band position in Fig. 5b determines the hypothetical ideal behavior of the DMSO–water solutions. It is obvious that the system is non-ideal. The inflection points of the discussed relationship suggest the existence of various molecular complexes. The first pronounced inflection point occurs at $x_w \simeq 0.4$, which corresponds to the 3DMSO·2H_2O complex. However, such complexes are highly labile and can form many structures in the solution (see Fig.S3 in the Supplementary Material). The representative 3DMSO·2H_2O complex is indicated in Fig. 4b. The next point is less marked and occurs at $x_w \simeq 0.85$. In this case, the stoichiometry of the complex is poorly defined and can be approximated by the set of complexes of the type 1DMSO·nH_2O, where $n = 4 \div 6$. To simplify further discussion, we will use the formula 1DMSO·4H_2O, which corresponds to the core structure of the nascent hydration shell around the hydrophobic groups of DMSO. The structure of such a complex is presented in Fig. 4c. The discussed complex still lacks hydrogen bonds between water molecules around the non-polar parts of DMSO molecule. Therefore, the strong hydrogen bonds in this complex, can be attributed to the water molecules interacting with the S=O group and correspond to the population of the O$\cdots$O distances characterized by the maximum at ca. 2.75 Å in $\Delta P(R_{OO})_{x=0.85}$, as shown in Fig. 2b. In the discussed complex a water cage is developed around the DMSO molecule. This expansion is confirmed by DFT calculations and presented in the form of various structures in Fig. S6 in the Supplementary Material. The formation of the water cage is also evidenced from AIMD simulations which confirm (by spatial distribution functions of water oxygens around DMSO, see Fig. S11) that the particular static structures from DFT calculations indeed correlate

with the average solvation structure of DMSO. The last point of inflection is very sharp and corresponds to $x_w \simeq 0.98$.

It is worth noting that the distinguished solution compositions (i.e. $x_w \simeq 0.4$ and $x_w \simeq 0.85$) correspond well to those observed for the HDO spectra in the range of the ν(OD) vibrations (section 3.1). Thus, changes in DMSO vibrational structure is highly correlated with changes in the arrangement of solvating water.

The results of the principal factor analysis (PFA algorithm) applied to the spectra in Fig. 5a lead to the conclusion that they can be adequately reproduced using four principal factors. This is also the number of absorbing species present in the solutions. By using the window factor analysis, the relative concentration profiles of these species were obtained and presented in Fig. 5c. It should be stressed that factor analysis confirmed the presence of molecular complexes in the tested solutions with compositions corresponding to the inflection points observed in Fig. 5b (black and blue). The first factor corresponding to ν(S=O) band (red) shows maximum intensity for pure DMSO and can be assigned to DMSO molecules that do not form hydrogen bonds with water. As it can be seen, the dependence of the relative contribution of this factor vs. x_w is qualitatively similar to the one obtained in a different way and presented in Fig. 5d (red). On the other hand, the assignment of the factor dominant in water-rich solutions (green) requires careful consideration. Its relative contribution can be qualitatively reconstructed by a similar procedure as in the case of the first factor. For this purpose, we analyzed the participation of the boundary spectrum at $x_w \simeq 0.98$ (with the highest intensity in Fig. 5a) in the spectra of water-rich mixtures. It must be

stressed, however, that this spectrum does not correspond to the infinitely diluted DMSO. It is only the closest approximation we were able to get, but the obtained contribution profile is reasonable and closely resembles the one calculated with chemometric algorithm. We attribute the fourth factor (green) to DMSO molecules that are able to embed via hydrogen bonds into a clathrate-like cage of water. The corresponding relationship in Fig. 5c shows the variability of the relative proportion of DMSO molecules in this state. It should be added here that the spectra that correspond to $x_w \gtrsim 0.98$ were assigned to DMSO molecules that are partly free from hydrogen bonds within the water cage and have gained some degree of rotational freedom.

Molecular complexes $3DMSO{\cdot}2H_2O$ and $1DMSO{\cdot}4H_2O$ are composed of the same molecules, so it can be expected that their enthalpy of mixing will be almost ideal or close to zero. However, they differ in size and, most importantly, in structure. Therefore, the non-ideality of the solution resulting from the mixing of such complexes will be reflected in the positive excess entropy, in accordance with the theory of athermal solutions developed by Huggins [92], Flory [93] and Miller [94]. Hence, a solution with a composition corresponding to equal relative contributions of both complexes, corresponding to $x_w = 0.67$ (marked with the red dashed line in Fig. 5c) should have the maximum entropy. This, in turn, translates into the minimum of the Gibbs free energy of such solution. Finally, it should consequently have a minimum temperature of solidification. In our opinion, the presented reasoning explains the occurrence of an eutectic point for the DMSO–water system at $x_w = 0.67$. Its appearance is thus of entropic nature and corresponds to the largest number of configurations responsible for the intermolecular interac-

tions between the highlighted molecular complexes. Previously, Kircher and Reiher [31] proposed a somewhat similar concept. Accordingly, in the eutectic mixture many energetically similar, but structurally different molecular complexes exist (proposed by the authors on the basis of *ab initio* calculations) that cannot easily transform their conformations into one another. It leads to the hindered formation of hydrogen bonds between clusters. We want to emphasize that on the basis of our results we see no premise for the existence of the 1DMSO·2H_2O molecular complex, often postulated by other authors (ref. [25] and references cited therein), which would justify the depression of melting point of the solutions at the discussed composition.

3.2.3. Spectra in the range of ν(C-H) vibrations

The asymmetric and symmetric ν(C-H) bands of DMSO methyl groups (located at 2996 ± 1 and 2912 ± 1 cm^{-1}, respectively, in the case of pure DMSO; data not shown) demonstrate a clear blue-shift of 22 and 12 cm^{-1}, respectively, as the water content in mixtures with DMSO increases. Such a shift corresponds to the formation of hydrogen bonds of the C-H$\cdots$$OH_2$ type between methyl groups of DMSO and lone electron pairs of water molecules [31, 95, 96, 97, 98, 99, 100]. The rate of the shift with increasing x_w clearly accelerates after exceeding $x_w \simeq 0.5$. The corresponding dependencies of the band shift on x_w can be found in previous works [95, 100]. It is important to note the change of the blue-shift into the red-shift for $x_w > 0.96$. We can associate this unexpected change in the direction of the band shift with the already discussed change of the behavior of the ν(S=O) band in a very similar range of compositions. Clearly, relatively weak hydrogen bonds of the C-H$\cdots$$OH_2$ type, which are two to four times weaker than water–water

hydrogen bonds [31, 97, 99], play a special or even a key role in the intermolecular interactions between DMSO and water. The high importance of such hydrogen bonds, disregarding their relatively weak character, stems from their non-negligible number: the analysis of AIMD simulations shows that almost 0.5 hydrogen bonds per C-H bond, and simultaneously 2.5 such bonds per DMSO molecule, are formed on average (see Figs. S8 and S9 in the Supplementary Material).

The role of C-H$\cdots$OH$_2$ "improper" hydrogen bonds becomes clear when the RDG method is applied to the electron densities calculated for DFT-optimized complexes of DMSO with different number of surrounding water molecules (including both low—classical DFT—and high—ONIOM-based—water content complexes). Such bonds are weaker than other hydrogen bonds, yet their orientation and localization between the hydrogen bond donor and acceptor are as good (Fig. 4). These bonds are present even in pure DMSO complexes and facilitate the self-association of molecules (Fig. 4a). When water molecules are introduced into the complex, such interactions become possible also between the oxygen atom of water molecules and methyl groups of DMSO (Fig. 4b). However, the most important role of such bonding is clearly visible when the number of water molecules is high enough to form an initial core structure of the future hydration shell (Fig. 4c). These hydrogen bonds impose the position of water molecules and stabilize the shell formation. The core is stabilized solely by proper and improper hydrogen bonds, and the van der Waals interactions are almost absent, even with 10 water molecules per one DMSO (Fig. 6a). These interactions, however, tend to substitute C-H$\cdots$OH$_2$ bonds when the number of water molecules is

high enough to almost cover one of the methyl groups, as in Fig. 6b. In this figure, two "improper" bonds are visible around the left CH_3 group, while the right one interacts with its hydration shell through van der Waals interactions marked with green/olive flat surfaces. In complexes with higher water content the, "improper" hydrogen bonds are almost absent and the hydrophobic part of the DMSO molecule is covered with patches of van der Waals interactions (Fig. 6c).

——Figure 6——

The change in the character of DMSO–water interactions is reflected also in the simple geometry of ONIOM-calculated complexes. When the hydration shell starts to cover the central DMSO molecule, more and more C–H bonds are released from the "improper" hydrogen bonds. Consequently, the mean C–H bond length is shortened (Fig. S4 in Supplementary Material), which translates into the blue-shift observed in the FTIR spectra. The process is stopped when the hydration shell is complete and such hydrogen bonds are no more present in the complexes. We note here that the complete hydration shell of DMSO at $x_w \simeq 0.988$ (the AIMD-studied system) contains on average 29.2 water molecules (see Fig. S10 and Table S2 in the Supplementary Material). The C–H bond length reaches minimum at ca. 30 water molecules per 1 DMSO and increases at higher water contents. We note here that this closely corresponds to the number of water molecules in the full hydration shell of DMSO, as evidenced by DMSO$\cdots$$D_2O$ radial distribution function obtained from AIMD simulations (see Fig. S10 and Table S2 in Supplementary Material). Moreover, the mean $C_{DMSO}\cdots O_{water}$ distance increases with the number of water molecules in the shell (Fig. S5 in Supple-

mentary Material). Such geometry change of the water cage around DMSO favors partial rotational freedom of the guest molecule inside, as suggested by FTIR spectra of DMSO in the range of ν(S=O) vibrations (see also section 3.2.1).

3.2.4. Increase of the rotational freedom of DMSO molecule in its water cage

It seems very likely that hydrogen bonding of the red-shifted and the blue-shifted types are cooperative according to refs [98, 99, 100]. It is also possible that DMSO is not an exception and other solutes, including biomolecules, can undergo a similar process. The way of formation of the hydration cage is generally consistent with the progressive hydration model proposed by Mrázková and Hobza [97]. The only caveat resulting from our research concerns the fact that the blue-shifted hydrogen bonds become less important when the construction of the water cage becomes fully complete and the cage itself becomes more relaxed.

The aforementioned weakening of the water hydrogen bonds with the S=O group of DMSO (section 3.2.1), progressing with the increasing size of the hydration complex, together with changes in the interaction of the water cage with DMSO molecule and the modification of the size of the cage itself (inferred from the DFT calculations presented in section 3.2.3) create conditions for the partial release of the DMSO molecule from the network of hydrogen bonds with water to a degree that allows a certain rotational freedom. This is supported by the spectral effects observed in Fig. 5a (blue lines) and the change of the blue-shift into the red-shift of the ν(C-H) DMSO bands [95, 100] taking place at the lowest DMSO concentrations. The driving force behind the observed phenomenon is the entropy gain associated with

the recovery of rotational freedom of the guest molecule.

We also note here that the formation of the water cage is connected with the orientational retardation of water molecules in the DMSO hydration shell, as clearly evidenced by the orientational relaxation time of the O–D bond of D_2O increasing from 2.3 ps in bulk water to 3.1 ps in the hydration shell, see the Supplementary Material for details.

3.3. Hydration of DMSO in the light of other water-soluble solutes regarded as "hydrophobic"

Recently, Grdadolnik *et al.* [13] have demonstrated, the presence of the ice-like hydration water around small purely hydrophobic solutes (i.e., methane, ethane, krypton, and xenon). Ice (Ih), solid clathrates of these substances and their solutions gave a single ν(OD) band of HDO at the same position, ca. 2440 ± 10 cm^{-1}, which corresponds to $R_{OO} = 2.76 \pm 0.01$ Å.

——Figure 7——

Substances included in Fig. 7 allow us to better justify the thesis that the hydration of DMSO in water-rich solutions is hydrophobic in nature, leading to the formation of a clathrate-like structure. Both the tetrabutylammonium cation (Bu_4N^+) and tetrahydrofuran (THF) form solid clathrates [103, 104, 105] and are commonly regarded as model hydrophobic molecules [105, 106, 44, 101]. The hydration sphere in both cases is composed of ice-like water molecules and the accompanying population of water molecules with O···O distances longer than in the bulk water. The latter often dominates and obscures the effect of the presence of "ice-like" water molecules [79]. However, among the solutes listed in Fig. 7, DMSO is characterized by a hydration sphere in which water molecules with the "ice-like" structure are dominant

($R_{OO} \simeq 2.75$ Å).

The use of differences between interatomic O···O distance distribution functions (Fig. 7b) is probably the most appropriate method for uncovering the presence of subtle and labile structures in solution. Simulation methods can also sometimes fail in this respect if we take into account the information resulting from the analysis of the affected spectra, regarding the affected number, N (note, however, that the normalization factor for the distance-dependent IR spectra derived from AIMD simulations often remains in close correspondence to the experimental N value, as found also in this work).

It can be estimated on the basis of Fig. 7b that within the hydration sphere of DMSO the contribution of "ice-like" water ($R_{OO} \simeq 2.75$ Å) relative to the water with a weakened structure ($R_{OO} \simeq 2.90$ Å) is close to 2/3. Taking into account the N value for the infinite dilution solution (2.8, see inset in Fig. 2a and Table S1 in Supplementary Material), we obtain ca. 2 water molecules which statistically form the ice-like structure in the hydration sphere of DMSO. However, we must take into account that about half of this population are water molecules that form hydrogen bonds with the DMSO oxygen atom (Fig. 2b). On the other hand, for Bu_4N^+ it can be estimated, basing on data in ref. [44], that N equals to ca. 3 and that the contribution of the "ice-like" water in the cation hydration sphere is close to 1/3 (Fig. 7), which indicates that statistically only 1 water molecule of the "ice-like" structure can be found in its hydration sphere. As it can be seen in Fig. 7b, THF ($N = 3.2$ [101]) lies between DMSO and Bu_4N^+ in respect of proportion of the "ice-like" water and the water with weakened structure. Therefore, for typical water-soluble small solutes that contain non-polar groups one can

expect on average one water molecule forming the "ice-like" structure.

In the light of the above-mentioned Grdadolnik's findings [13], the question arises about the origin of the accompanying population of water molecules with weakened hydrogen bonding in the case of hydrophobic water-soluble molecules. The formal answer to this question arises from simple thermodynamic predictions. Because the formation of the "iceberg", triggered by the presence of the solute, is very entropy consuming and leads to a low solubility of such solute, any other structural opportunity for water molecules which is less "structured" will be more thermodynamically favorable and improve the solubility in water. An explanation on the molecular level should take into account also molecular premises. It should be noted that in the case of Bu_4N^+ cation the solvent accessible surface consists of convex and concave areas. Water molecules in the surroundings of the convex area have a chance to build a network of ice-type hydrogen bonds with an approximately parallel molecule orientation relative to the surface. On the other hand, in the concave areas the probability of perpendicular orientation of water molecules, i.e. with their lone electron pairs pointing towards the hydrophobic surface, is growing. As has been discussed in the Supplementary Material (section S1.3), water molecules which do not engage their lone electron pairs in classical hydrogen bonds are less polarized and exhibit a blue-shifted ν(OD/OH) band. According to this argumentation, those water molecules which are in the concave areas of the Bu_4N^+ cation should contribute to the population of molecules with "weakened hydrogen bonds". Those molecules which are in the vicinity of convex areas should have contribute to the population of the ice-like water molecules. In the case of DMSO, the accompanying population

of molecules with weakened hydrogen bonds originate from improper fit of water molecules hydrogen bonded to the oxygen atom of DMSO, to the bulk water, as recognized in this work from AIMD simulations. In the case of THF hydration, it can be presumed that the source of water molecules with weakened hydrogen bonds is similar in nature to the DMSO case.

4. Conclusions

DMSO-water mixtures have been studied by means of the FTIR spectroscopy in the range of DMSO vibration and HDO stretching vibrations (as a probe of hydration water) in the whole range of mixture compositions. Theoretical calculations facilitated the interpretation of experimental results. This helped us to redefine the view on the hydration of DMSO.

It has been established that in diluted solutions of DMSO the clathrate-like water cage is created around the DMSO molecule. The formation of this cage is facilitated by interactions between water molecules and methyl groups of the guest molecule (the blue-shifted hydrogen bonds) and it is particularly evidenced by the spatial distribution function of water around DMSO that clearly displays the emergence of cage structures around methyl groups. For even more diluted solutions, when the water cage is fully completed, the DMSO molecule partly regains its rotational freedom inside. The driving force behind this effect is the entropy gain. Weakened hydrogen bonds of water molecules population arise from those water molecules which are hydrogen bonded to the ones already interacting with the oxygen atom of DMSO. Most probably, it happens because strong hydrogen bonds of water molecules directly bonded to the hydrophilic group of the solute poorly fit

to the structure of the bulk water. This population with weakened hydrogen bonds efficiently obscures the presence of the population with strong hydrogen bonds formed with the SO group of DMSO and between water molecules around the methyl groups in the overall spectral effect. We also propose a novel explanation of the strong deviation from ideality of DMSO-water mixtures at composition corresponding to the eutectic point of the system. Namely, it stems from an equimolar mixture of the molecular complexes of the $3DMSO{\cdot}2H_2O$ and of $1DMSO{\cdot}nH_2O$ ($n = 4 \div 6$) type. For such a mixing the, maximum excess entropy is expected, which justifies the depression of the melting point of the solution at $x_w = 0.67$.

5. Acknowledgements

J. S. would like to thank Dr. Ewa Kamieńska-Piotrowicz for her help in experiment. Calculations were carried out at the Academic Computer Centre in Gdańsk.

6. Declaration of interest

The authors declare that they have no conflict of interest.

[1] P. Ball, Water is an active matrix of life for cell and molecular biology., Proceedings of the National Academy of Sciences of the United States of America 114 (2017) 13327–13335.

[2] W. Kauzmann, Some Factors in the Interpretation of Protein Denaturation, Advances in Protein Chemistry 14 (1959) 1–63.

[3] C. Tanford, The hydrophobic effect and living matter, Science 200 (1978) 1012–1018.

[4] M. Charton, B. I. Charton, The structural dependence of amino acid hydrophobicity parameters, Journal of Theoretical Biology 99 (1982) 629–644.

[5] R. L. Baldwin, Temperature dependence of the hydrophobic interaction in protein folding., Proceedings of the National Academy of Sciences 83 (1986) 8069–8072.

[6] K. A. Dill, Dominant forces in protein folding, Biochemistry 29 (1990) 7133–7155.

[7] W. Blokzijl, J. B. Engberts, Hydrophobic Effects. Opinions and Facts, Angewandte Chemie International Edition in English 32 (1993) 1545–1579.

[8] V. R. Agashe, M. C. R. Shastry, J. B. Udgaonkar, Initial hydrophobic collapse in the folding of barstar, Nature 377 (1995) 754–757.

[9] H. J. Dyson, P. E. Wright, H. A. Scheraga, The role of hydrophobic interactions in initiation and propagation of protein folding, Proceedings of the National Academy of Sciences 103 (2006) 13057–13061.

[10] P. Ball, Water as an Active Constituent in Cell Biology, Chemical Reviews 108 (2008) 74–108.

[11] H. S. Frank, M. W. Evans, Free Volume and Entropy in Condensed Systems III. Entropy in Binary Liquid Mixtures; Partial Molal En-

tropy in Dilute Solutions; Structure and Thermodynamics in Aqueous Electrolytes, The Journal of Chemical Physics 13 (1945) 507–532.

[12] T. Hajari, S. Bandyopadhyay, Water structure around hydrophobic amino acid side chain analogs using different water models, The Journal of Chemical Physics 146 (2017) 225104.

[13] J. Grdadolnik, F. Merzel, F. Avbelj, Origin of hydrophobicity and enhanced water hydrogen bond strength near purely hydrophobic solutes, Proceedings of the National Academy of Sciences 114 (2017) 322–327.

[14] D. T. Bowron, A. Filipponi, M. A. Roberts, J. L. Finney, Hydrophobic Hydration and the Formation of a Clathrate Hydrate, Physical Review Letters 81 (1998) 4164–4167.

[15] N. Uras-Aytemiz, I. Abrrey Monreal, J. P. Devlin, Communication: Quantitative Fourier-transform infrared data for competitive loading of small cages during all-vapor instantaneous formation of gas-hydrate aerosols, Journal of Chemical Physics 135 (2011) 2–5.

[16] J. L. Finney, Overview lecture. Hydration processes in biological and macromolecular systems, Faraday Discussions 103 (1996) 1.

[17] A. K. Soper, Neutron scattering studies of solvent structure in systems of chemical and biological importance, Faraday Discussions 103 (1996) 41.

[18] D. Martin, A. Weise, H.-J. Niclas, The Solvent Dimethyl Sulfoxide, Angewandte Chemie International Edition in English 6 (1967) 318–334.

[19] U. Kaatze, R. Pottel, M. Schaefer, Dielectric spectrum of dimethyl sulfoxide/water mixtures as a function of composition, The Journal of Physical Chemistry 93 (1989) 5623–5627.

[20] Z. Lu, E. Manias, M. Lanagan, D. Macdonald, Dielectric Relaxation in Dimethyl Sulfoxide/Water Mixtures, ECS Transactions 28 (2010) 11–21.

[21] S. Y. Lam, R. L. Benoit, Some Thermodynamic Properties of the Dimethylsulfoxide–Water and Propylene Carbonate–Water Systems at 25°C, Canadian Journal of Chemistry 52 (1974) 718–722.

[22] J. T. Cabral, A. Luzar, J. Teixeira, M.-C. Bellissent-Funel, Single-particle dynamics in dimethyl–sulfoxide/water eutectic mixture by neutron scattering, The Journal of Chemical Physics 113 (2000) 8736.

[23] I. A. Borin, M. S. Skaf, Molecular association between water and dimethyl sulfoxide in solution: A molecular dynamics simulation study, The Journal of Chemical Physics 110 (1999) 6412–6420.

[24] P. P. Wiewiór, H. Shirota, E. W. Castner, Aqueous dimethyl sulfoxide solutions: Inter- and intra-molecular dynamics, The Journal of Chemical Physics 116 (2002) 4643–4654.

[25] V. M. Wallace, N. R. Dhumal, F. M. Zehentbauer, H. J. Kim, J. Kiefer, Revisiting the Aqueous Solutions of Dimethyl Sulfoxide by Spectroscopy in the Mid- and Near-Infrared: Experiments and Car–Parrinello Simulations, The Journal of Physical Chemistry B 119 (2015) 14780–14789.

[26] J. M. G. Cowie, P. M. Toporowski, Association in the binary liquid system dimethyl sulphoxide-water, Canadian Journal of Chemistry 39 (1961) 2240–2243.

[27] S. S. N. Murthy, Phase Behavior of the Supercooled Aqueous Solutions of Dimethyl Sulfoxide, Ethylene Glycol, and Methanol As Seen by Dielectric Spectroscopy, The Journal of Physical Chemistry B 101 (1997) 6043–6049.

[28] I. I. Vaisman, M. L. Berkowitz, Local structural order and molecular associations in water-DMSO mixtures. Molecular dynamics study, Journal of the American Chemical Society 114 (1992) 7889–7896.

[29] I. A. Borin, M. S. Skaf, Molecular association between water and dimethyl sulfoxide in solution: the librational dynamics of water, Chemical Physics Letters 296 (1998) 125–130.

[30] A. Vishnyakov, A. P. Lyubartsev, A. Laaksonen, Molecular Dynamics Simulations of Dimethyl Sulfoxide and Dimethyl Sulfoxide-Water Mixture, The Journal of Physical Chemistry A 105 (2001) 1702–1710.

[31] B. Kirchner, M. Reiher, The Secret of Dimethyl Sulfoxide-Water Mixtures. A Quantum Chemical Study of 1DMSO- n Water Clusters, Journal of the American Chemical Society 124 (2002) 6206–6215.

[32] G. J. Safford, P. C. Schaffer, P. S. Leung, G. F. Doebbler, G. W. Brady, E. F. X. Lyden, Neutron Inelastic Scattering and X-Ray Studies of Aqueous Solutions of Dimethylsulphoxide and Dimethylsulphone, The Journal of Chemical Physics 50 (1969) 2140–2159.

[33] D. H. Rasmussen, A. P. MacKenzie, Phase Diagram for the System Water–Dimethylsulphoxide, Nature 220 (1968) 1315–1317.

[34] E. S. Baker, J. Jonas, Transport and relaxation properties of dimethyl sulfoxide-water mixtures at high pressure, The Journal of Physical Chemistry 89 (1985) 1730–1735.

[35] A. K. Soper, A. Luzar, Orientation of Water Molecules around Small Polar and Nonpolar Groups in Solution: A Neutron Diffraction and Computer Simulation Study, The Journal of Physical Chemistry 100 (1996) 1357–1367.

[36] Y. Koga, Y. Kasahara, K. Yoshino, K. Nishikawa, Mixing Schemes for Aqueous Dimethyl Sulfoxide: Support by X-ray Diffraction Data, Journal of Solution Chemistry 30 (2001) 885–893.

[37] Z. S. Klemenkova, E. G. Kononova, Elucidation of the Water–DMSO Mixing Process Based on an IR Study, Journal of Solution Chemistry 44 (2015) 280–292.

[38] R. L. Mancera, M. Chalaris, K. Refson, J. Samios, Molecular dynamics simulation of dilute aqueous DMSO solutions. A temperature-dependence study of the hydrophobic and hydrophilic behaviour around DMSO, Physical Chemistry Chemical Physics 6 (2004) 94.

[39] R. L. Mancera, M. Chalaris, J. Samios, The concentration effect on the 'hydrophobic' and 'hydrophilic' behaviour around DMSO in dilute aqueous DMSO solutions. A computer simulation study, Journal of Molecular Liquids 110 (2004) 147–153.

817 [40] K. Subbarangaiah, N. M. Murthy, S. V. Subrahmanyam, Ultra-
818 sonic Investigation on the Structure of Aqueous Solutions of *N,N*-
819 Dimethylformamide and Dimethyl Sulfoxide, Bulletin of the Chemical
820 Society of Japan 54 (1981) 2200–2204.

821 [41] G. Petrella, M. Petrella, M. Castagnolo, A. Dell'Atti, A. De Giglio,
822 Solute-Solvent interactions in water-rich mixtures. II. Ionic conduc-
823 tances in water-dimethylsulfoxide mixtures at 25°C, Journal of Solu-
824 tion Chemistry 10 (1981) 129–138.

825 [42] A. Panuszko, P. Bruździak, E. Kaczkowska, J. Stangret, General Mech-
826 anism of Osmolytes' Influence on Protein Stability Irrespective of the
827 Type of Osmolyte Cosolvent, The Journal of Physical Chemistry B
828 120 (2016) 11159–11169.

829 [43] J. Stangret, Solute-Affected Vibrational Spectra of Water in $Ca(ClO_4)_2$
830 Aqueous Solutions, Spectroscopy Letters 21 (1988) 369–381.

831 [44] J. Stangret, T. Gampe, Hydration Sphere of Tetrabutylammonium
832 Cation. FTIR Studies of HDO Spectra, The Journal of Physical Chem-
833 istry B 103 (1999) 3778–3783.

834 [45] M. Śmiechowski, J. Stangret, Vibrational spectroscopy of semiheavy
835 water (HDO) as a probe of solute hydration, Pure and Applied Chem-
836 istry 82 (2010) 1869–1887.

837 [46] E. Malinowski, Factor Analysis in Chemistry, Wiley, New York, 2002.

838 [47] E. R. Malinowski, Window factor analysis: Theoretical derivation and

application to flow injection analysis data, Journal of Chemometrics 6 (1992) 29–40.

[48] M. J. Frisch, G. W. Trucks, H. B. Schlegel, G. E. Scuseria, M. A. Robb, J. R. Cheeseman, G. Scalmani, V. Barone, B. Mennucci, G. A. Petersson, H. Nakatsuji, M. Caricato, X. Li, H. P. Hratchian, A. F. Izmaylov, J. Bloino, G. Zheng, J. L. Sonnenberg, M. Hada, M. Ehara, K. Toyota, R. Fukuda, J. Hasegawa, M. Ishida, T. Nakajima, Y. Honda, O. Kitao, H. Nakai, T. Vreven, J. A. Montgomery Jr., J. E. Peralta, F. Ogliaro, M. Bearpark, J. J. Heyd, E. Brothers, K. N. Kudin, V. N. Staroverov, R. Kobayashi, J. Normand, K. Raghavachari, A. Rendell, J. C. Burant, S. S. Iyengar, J. Tomasi, M. Cossi, N. Rega, J. M. Millam, M. Klene, J. E. Knox, J. B. Cross, V. Bakken, C. Adamo, J. Jaramillo, R. Gomperts, R. E. Stratmann, O. Yazyev, A. J. Austin, R. Cammi, C. Pomelli, J. W. Ochterski, R. L. Martin, K. Morokuma, V. G. Zakrzewski, G. A. Voth, P. Salvador, J. J. Dannenberg, S. Dapprich, A. D. Daniels, Ö. Farkas, J. B. Foresman, J. V. Ortiz, J. Cioslowski, D. J. Fox, Gaussian 09, Revision D.01, 2009.

[49] E. R. Johnson, S. Keinan, P. Mori-Sanchez, J. Contreras-Garcia, A. J. Cohen, W. Yang, Revealing noncovalent interactions, Journal of the American Chemical Society 132 (2010) 6498–6506.

[50] T. Lu, F. Chen, Multiwfn: A multifunctional wavefunction analyzer, Journal of Computational Chemistry 33 (2012) 580–592.

[51] S. Grimme, S. Ehrlich, L. Goerigk, Effect of the damping function in

dispersion corrected density functional theory, Journal of Computational Chemistry 32 (2011) 1456–1465.

[52] C. Lee, W. Yang, R. G. Parr, Development of the Colle-Salvetti correlation-energy formula into a functional of the electron density, Phys. Rev. B 37 (1988) 785–789.

[53] A. D. Becke, Density-functional thermochemistry. III. the role of exact exchange, The Journal of Chemical Physics 98 (1993) 5648–5652.

[54] R. Ditchfield, W. J. Hehre, J. A. Pople, Self-consistent molecular-orbital methods. IX. an extended gaussian-type basis for molecular-orbital studies of organic molecules, The Journal of Chemical Physics 54 (1971) 724–728.

[55] V. Barone, M. Cossi, Quantum calculation of molecular energies and energy gradients in solution by a conductor solvent model, Journal of Physical Chemistry A 102 (1998) 1995–2001.

[56] M. Cossi, N. Rega, G. Scalmani, V. Barone, Energies, structures, and electronic properties of molecules in solution with the C-PCM solvation model, Journal of Computational Chemistry 24 (2003) 669–681.

[57] V. P. Ananikov, D. G. Musaev, K. Morokuma, Real size of ligands, reactants and catalysts: Studies of structure, reactivity and selectivity by ONIOM and other hybrid computational approaches, Journal of Molecular Catalysis A: Chemical 324 (2010) 104–119.

[58] T. A. Halgren, Merck molecular force field. I. Basis, form, scope, parameterization, and performance of MMFF94, J. Comput. Chem. 17 (1996) 490–519.

[59] T. A. Halgren, Merck molecular force field. II. MMFF94 van der Waals and electrostatic parameters for intermolecular interactions, J. Comput. Chem. 17 (1996) 520–552.

[60] D. Marx, J. Hutter, Ab Initio Molecular Dynamics, Cambridge University Press, Cambridge, 2009.

[61] J. VandeVondele, M. Krack, F. Mohamed, M. Parrinello, T. Chassaing, J. Hutter, Quickstep: Fast and accurate density functional calculations using a mixed Gaussian and plane waves approach, Computer Physics Communications 167 (2005) 103–128.

[62] The `cp2k` Developers Group, `cp2k` v. 6.0, 2001–2018. `http://www.cp2k.org/`.

[63] J. Hutter, M. Iannuzzi, F. Schiffmann, J. VandeVondele, cp2k: atomistic simulations of condensed matter systems, WIREs Comput. Mol. Sci. 4 (2014) 15–25.

[64] A. D. Becke, Density-functional exchange-energy approximation with correct asymptotic behavior, Phys. Rev. A 38 (1988) 3098–3100.

[65] S. Grimme, J. Antony, S. Ehrlich, H. Krieg, A consistent and accurate *ab initio* parametrization of density functional dispersion correction (DFT-D) for the 94 elements H-Pu, J. Chem. Phys. 132 (2010) 154104.

[66] G. Lippert, J. Hutter, M. Parrinello, A hybrid Gaussian and plane wave density functional scheme, Mol. Phys. 92 (1997) 477–487.

[67] S. Goedecker, M. Teter, J. Hutter, Separable dual-space Gaussian pseudopotentials, Phys. Rev. B 54 (1996) 1703–1710.

[68] M. Nakamura, K. Tamura, S. Murakami, Isotope effects on thermodynamic properties: mixtures of x(D_2O or H_2O) + (1-x)CH_3CN at 298.15 K, Thermochim. Acta 253 (1995) 127–136.

[69] R. B. Torres, P. L. O. V. A. C. M. Marchiore, Volumetric properties of binary mixtures of (water + organic solvents) at temperatures between T = 288.15 K and T = 303.15 K at p = 0.1 MPa, J. Chem. Thermodynamics 38 (2006) 526–541.

[70] I.-F. W. Kuo, C. J. Mundy, M. J. McGrath, J. I. Siepmann, J. VandeVondele, M. Sprik, J. Hutter, B. Chen, M. L. Klein, F. Mohamed, M. Krack, M. Parrinello, Liquid Water from First Principles: Investigation of Different Sampling Approaches, J. Phys. Chem. B 108 (2004) 12990–12998.

[71] T. Bryk, A. P. Seitsonen, Ab initio molecular dunamics study of collective excitations in liquid H_2O and D_2O: Effect of dispersion corrections, Condens. Matter Phys. 19 (2016) 1–14.

[72] G. J. Martyna, M. L. Klein, M. Tuckerman, Nosé–Hoover chains: The canonical ensemble via continuous dynamics, J. Chem. Phys. 97 (1992) 2635–2643.

[73] N. Marzari, D. Vanderbilt, Maximally localized generalized Wannier functions for composite energy bands, Phys. Rev. B 56 (1997) 12847–12865.

[74] M. Thomas, M. Brehm, R. Fligg, P. Vöringer, B. Kirchner, Computing vibrational spectra from ab initio molecular dynamics, Phys. Chem. Chem. Phys. 15 (2013) 6608–6622.

[75] M. Śmiechowski, J. Sun, H. Forbert, D. Marx, Solvation shell resolved THz spectra of simple aqua ions – distinct distance- and frequency-dependent contributions of solvation shells, Phys. Chem. Chem. Phys. 17 (2015) 8323–8329.

[76] M. Śmiechowski, Unusual Influence of the Fluorinated Anions on the Stretching Vibrations of Liquid Water, J. Phys. Chem. B 122 (2018) 3141–3152.

[77] H. Odhner, D. T. Jacobs, Refractive Index of Liquid D_2O for Visible Wavelengths, J. Chem. Eng. Data 57 (2012) 166–168.

[78] J. Stangret, Donor properties of water in organic solvents derived from infrared spectra of HDO, Journal of Molecular Structure 643 (2002) 29–35.

[79] E. Gojło, T. Gampe, J. Krakowiak, J. Stangret, Hydration of Aprotic Donor Solvents Studied by Means of FTIR Spectroscopy, The Journal of Physical Chemistry A 111 (2007) 1827–1834.

[80] J. E. Bertie, M. K. Ahmed, H. H. Eysel, Infrared intensities of liquids. 5. Optical and dielectric constants, integrated intensities, and dipole

moment derivatives of H_2O and D_2O at 22 °C, J. Phys. Chem. 93 (1989) 2210–2218.

[81] M. Heyden, J. Sun, S. Funkner, G. Mathias, H. Forbert, M. Havenith, D. Marx, Dissecting the THz spectrum of liquid water from first principles via correlations in time and space, Proc. Natl. Acad. Sci. USA 107 (2010) 12068–12073.

[82] L. R. Pestana, N. Mardirossian, M. Head-Gordon, T. Head-Gordon, Ab initio molecular dynamics simulations of liquid water using high quality meta-GGA functionals, Chem. Sci. 8 (2017) 3554–3565.

[83] O. Marsalek, T. E. Markland, Quantum Dynamics and Spectroscopy of Ab Initio Liquid Water: The Interplay of Nuclear and Electronic Quantum Effects, J. Phys. Chem. Lett. 8 (2017) 1545–1551.

[84] M. Leśniewski, M. Śmiechowski, Communication: Inside the water wheel: Intrinsic differences between hydrated tetraphenylphosphonium and tetraphenylborate ions, J. Chem. Phys. 149 (2018) 171101.

[85] S. Imoto, H. Forbert, D. Marx, Aqueous TMAO solutions as seen by theoretical THz spectroscopy: hydrophilic versus hydrophobic water, Phys. Chem. Chem. Phys. 20 (2018) 6146–6158.

[86] W. N. Martens, R. L. Frost, J. Kristof, J. Theo Kloprogge, Raman spectroscopy of dimethyl sulphoxide and deuterated dimethyl sulphoxide at 298 and 77 K, Journal of Raman Spectroscopy 33 (2002) 84–91.

[87] M.-T. Forel, M. Tranquille, Spectres de vibration du diméthylsulfoxyde

et dn diméthylsulfoxyde-d6, Spectrochimica Acta Part A: Molecular Spectroscopy 26 (1970) 1023–1034.

[88] W. R. Fawcett, A. A. Kloss, Solvent-Induced Frequency Shifts in the Infrared Spectrum of Dimethyl Sulfoxide in Organic Solvents, The Journal of Physical Chemistry 100 (1996) 2019–2024.

[89] K.-I. Oh, K. Rajesh, J. F. Stanton, C. R. Baiz, Quantifying Hydrogen-Bond Populations in Dimethyl Sulfoxide/Water Mixtures, Angew. Chem. Int. Ed. 56 (2017) 11375–11379.

[90] M. Y. Skripkin, P. Lindqvist-Reis, A. Abbasi, J. Mink, I. Persson, M. Sandström, Vibrational spectroscopic force field studies of dimethyl sulfoxide and hexakis(dimethyl sulfoxide)scandium(III) iodide, and crystal and solution structure of the hexakis(dimethyl sulfoxide)scandium(III) ion, Dalton Trans. 0 (2004) 4038–4049.

[91] N. S. Venkataramanan, A. Suvitha, Nature of bonding and cooperativity in linear DMSO clusters: A DFT, AIM and NCI analysis, Journal of Molecular Graphics and Modelling 81 (2018) 50–59.

[92] M. L. Huggins, Thermodynamic Properties of Solutions of Long Chain Compounds, Annals of the New York Academy of Sciences 43 (1942) 1–32.

[93] P. J. Flory, Thermodynamics of High Polymer Solutions, The Journal of Chemical Physics 10 (1942) 51–61.

[94] A. R. Miller, The Vapour-Pressure Equations of Solutions and the Osmotic Pressure of Rubber, Mathematical Proceedings of the Cambridge Philosophical Society 39 (1943) 54.

[95] K. Mizuno, S. Imafuji, T. Ochi, T. Ohta, S. Maeda, Hydration of the CH Groups in Dimethyl Sulfoxide Probed by NMR and IR, The Journal of Physical Chemistry B 104 (2000) 11001–11005.

[96] H.-C. Chang, J.-C. Jiang, C.-M. Feng, Y.-C. Yang, C.-C. Su, P.-J. Chang, S. H. Lin, High-pressure spectroscopic probe of hydrophobic hydration of the methyl groups in dimethyl sulfoxide, The Journal of Chemical Physics 118 (2003) 1802–1807.

[97] E. Mrázková, P. Hobza, Hydration of Sulfo and Methyl Groups in Dimethyl Sulfoxide Is Accompanied by the Formation of Red-Shifted Hydrogen Bonds and Improper Blue-Shifted Hydrogen Bonds: An ab Initio Quantum Chemical Study, The Journal of Physical Chemistry A 107 (2003) 1032–1039.

[98] L. Qingzhong, N. Wang, Y. Zhiwu, Effect of hydration on the C-H···O hydrogen bond: A theoretical study, Journal of Molecular Structure: THEOCHEM 847 (2007) 68–74.

[99] Q. Li, X. An, B. Gong, J. Cheng, Spectroscopic and theoretical evidence for the cooperativity between red-shift hydrogen bond and blue-shift hydrogen bond in DMSO aqueous solutions, Spectrochimica Acta Part A: Molecular and Biomolecular Spectroscopy 69 (2008) 211–215.

[100] Q. Li, X. An, B. Gong, J. Cheng, Comparison of contribution of OH···OS hydrogen bond and CH···O_w interaction to the methyl blueshift in hydration of dimethyl sulfoxide, Vibrational Spectroscopy 46 (2008) 28–33.

[101] J. Stangret, T. Gampe, Hydration of tetrahydrofuran derived from FTIR spectroscopy, Journal of Molecular Structure 734 (2005) 183–190.

[102] A. Panuszko, E. Gojło, J. Zielkiewicz, M. Śmiechowski, J. Krakowiak, J. Stangret, Hydration of Simple Amides. FTIR Spectra of HDO and Theoretical Studies, The Journal of Physical Chemistry B 112 (2008) 2483–2493.

[103] R. McMullan, G. A. Jeffrey, Hydrates of the Tetra *n*-butyl and Tetra *i*-amyl Quaternary Ammonium Salts, The Journal of Chemical Physics 31 (1959) 1231–1234.

[104] R. K. McMullan, M. Bonamico, G. A. Jeffrey, Polyhedral Clathrate Hydrates. V. Structure of the Tetra-*n*-butyl Ammonium Fluoride Hydrate, The Journal of Chemical Physics 39 (1963) 3295–3310.

[105] M. Bach-Vergés, S. J. Kitchin, K. D. M. Harris, M. Zugic, C. A. Koh, Dynamic Properties of the Tetrahydrofuran Clathrate Hydrate, Investigated by Solid State 2 H NMR Spectroscopy, The Journal of Physical Chemistry B 105 (2001) 2699–2706.

[106] W.-Y. Wen, Aqueous solutions of symmetrical tetraalkylammonium

salts, in: R. A. Horne (Ed.), Water and Aqueous Solutions, Wiley-Interscience, New York, 1972, pp. 613–661.

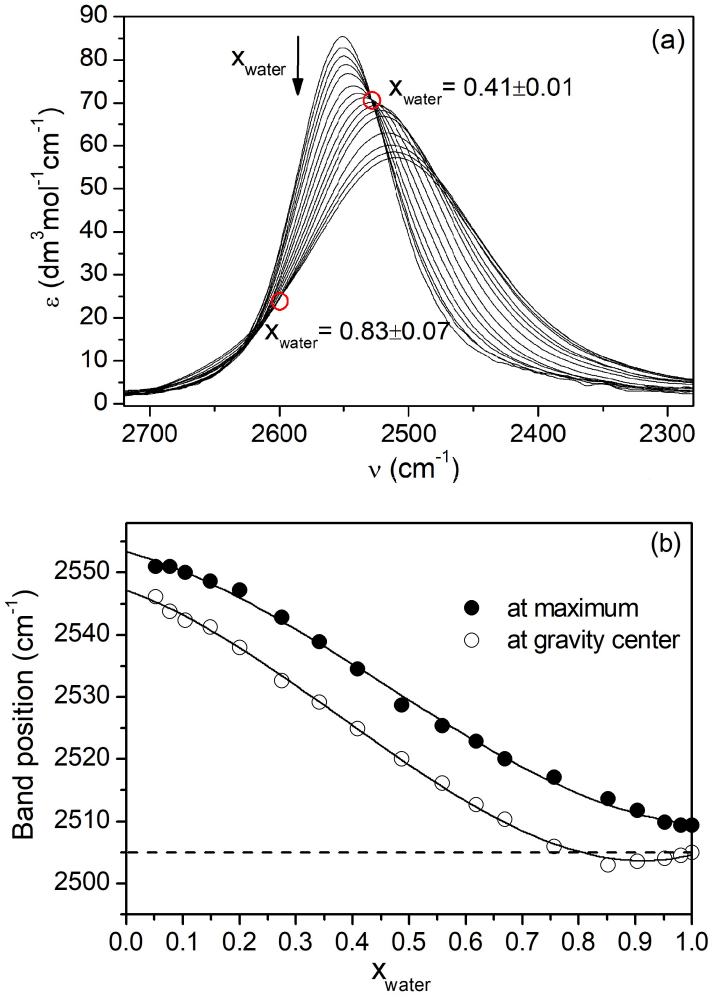

Figure 1: (a) Measured FTIR spectra of DMSO–water solutions at different mole fractions of water in the ν(OD) stretching vibrations range. The arrow shows increasing water mole fraction in the mixture. Red circles represent isosbestic points together with the corresponding water mole fractions: $x_w = 0.41 \pm 0.01$ (the maximum mole fraction to which the spectra intersect) and $x_w = 0.83 \pm 0.07$ (the minimum mole fraction from which the spectra begin to intersect). (b) The dependence of HDO band parameters on the mole fraction of water in the DMSO–water solutions. The dashed horizontal line denotes the band position at gravity center for pure water spectrum. Solid lines suggest the approximate relationship.

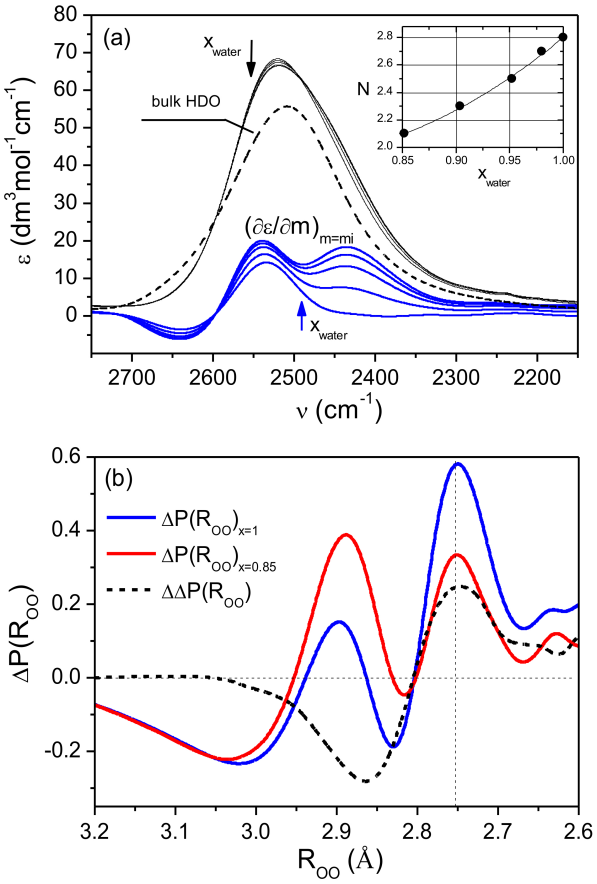

Figure 2: (a) DMSO–affected HDO spectra for high water content in mixtures, including the DMSO–affected HDO spectrum at the infinite dilution, for the water mole fractions as indicated in the inset (solid lines), along with the bulk HDO spectrum (black, dashed). Blue lines represent the derivatives $(d\varepsilon(\nu)/dm)_{m=m_i}$ for aqueous solutions of DMSO with molalities corresponding to the water mole fractions as indicated in the inset. The arrows indicate the direction of change of x_w in the mixture. Insert: The dependence of affected number, N, on the water mole fraction in the mixtures with the high water content. (b) Difference between interatomic oxygen-oxygen distance distribution function of DMSO-affected water at infinite dilution and the bulk water, (obtained on the basis of the spectra shown in Fig. 2a), $\Delta P(R_{OO})_{\mathrm{x=1}}$, and the corresponding distance difference for the DMSO-affected water for high water content ($x_w \simeq 0.85$) in the mixture (obtained on the basis of spectra in Fig. 2a), $\Delta P(R_{OO})_{\mathrm{x=0.85}}$. The black dashed line shows the difference: $\Delta\Delta P(R_{OO}) = \Delta P(R_{OO})_{\mathrm{x=1}} - \Delta P(R_{OO})_{\mathrm{x=0.85}}$. The vertical dashed line corresponds to the oxygen-oxygen distance in ice-like water (2.76 ± 0.01 Å).

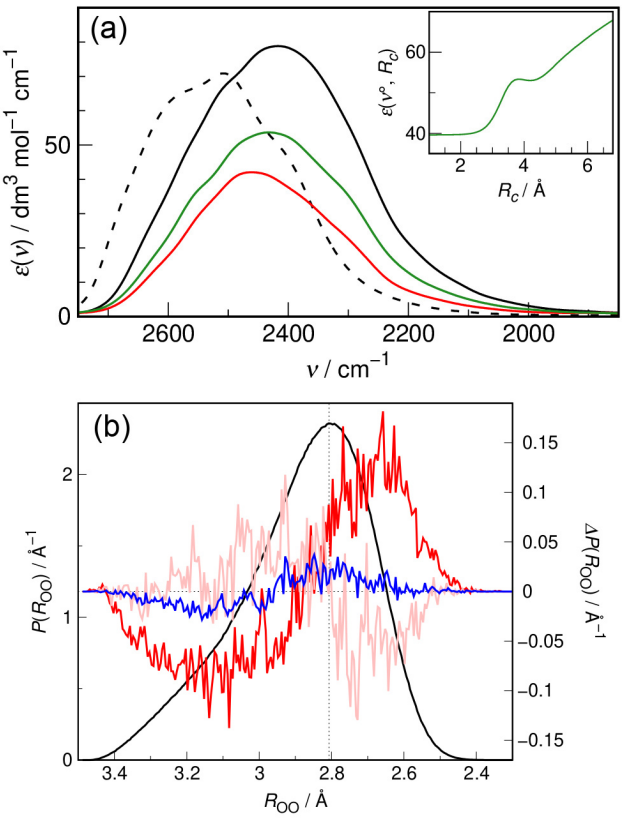

Figure 3: (a) Distance-dependent IR spectra from AIMD simulations at the cutoff radius $R_c \to 0$ (i.e., DMSO molecule extracted from the solution, red) and $R_c = 3.8$ Å (green), together with the bulk D_2O spectrum (black) and the experimental IR spectrum of pure liquid D_2O (ref [80], black dashed). The inset shows the dependence of the intensity of the distance-dependent IR spectrum on R_c at the probing wavenumber $\nu^\circ = 2461$ cm^{-1} (the position of the maximum at $R_c \to 0$). (b) The interatomic oxygen–oxygen distance distribution function for hydrogen bonded water molecules in bulk D_2O (black, left ordinate axis), $P(R_{OO})$, together with the distance differences with respect to bulk D_2O (right ordinate axis), $\Delta P(R_{OO})$, for: water–water hydrogen bonds in the hydration shell of methyl groups of DMSO (up to 4.7 Å, blue, cf. Fig. S10 and Table S2 in the Supplementary Material), water–water hydrogen bonds to water hydrogen bonded to the DMSO oxygen (up to 3.5 Å, pink), as well as water–DMSO oxygen hydrogen bonds (red). See section S4.1 in the Supplementary Material for hydrogen bond definitions. The vertical dashed line corresponds to the oxygen–oxygen distance in bulk D_2O ($R_{OO} \simeq 2.8$ Å).

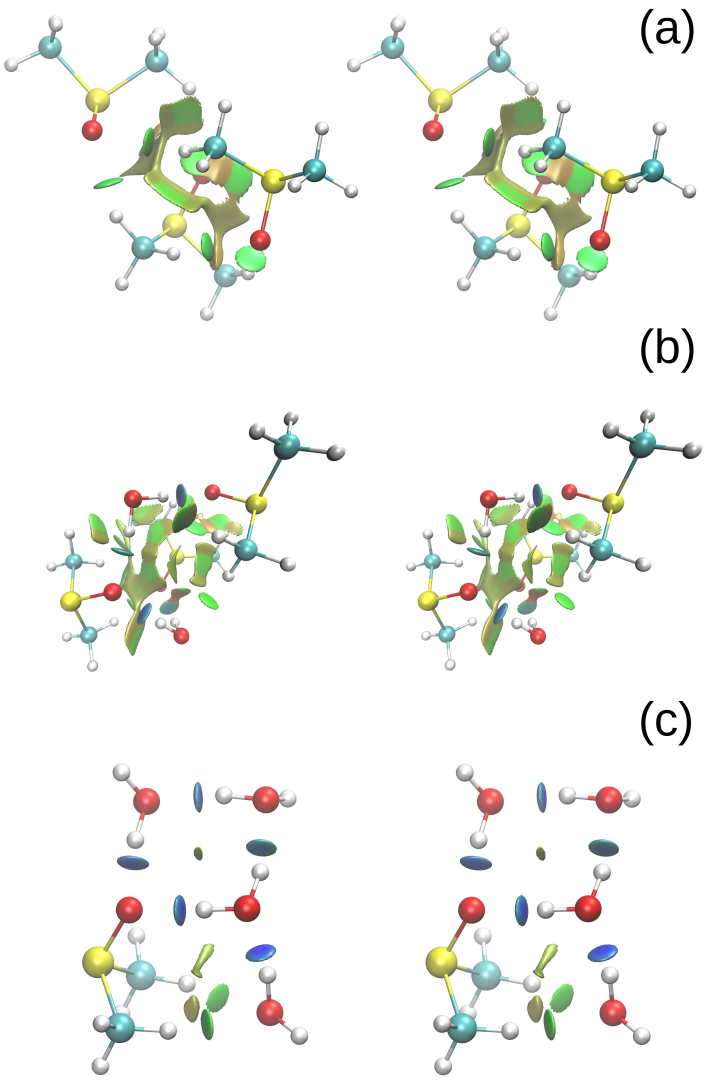

Figure 4: Stereo images of the results of weak interaction analysis of RDG function for (a) 3DMSO and small DMSO–water complexes: (b) 3DMSO·2H_2O, chosen on the basis of the course of changes in the shape of SO band and results of WFA analysis, and (c) 1DMSO·4H_2O, the first step of hydration sphere formation (the core type complex). Brown/olive flat, shapeless or elongated patches indicate van der Waals interactions, blue/green disks correspond to the hydrogen bonds (light green – weak HB, blue – strong HB). RDG calculated on the basis of electron densities obtained for DFT-optimized complexes in the CPCM model (B3LYP/6-311++G(d,p)). See explanation in text.

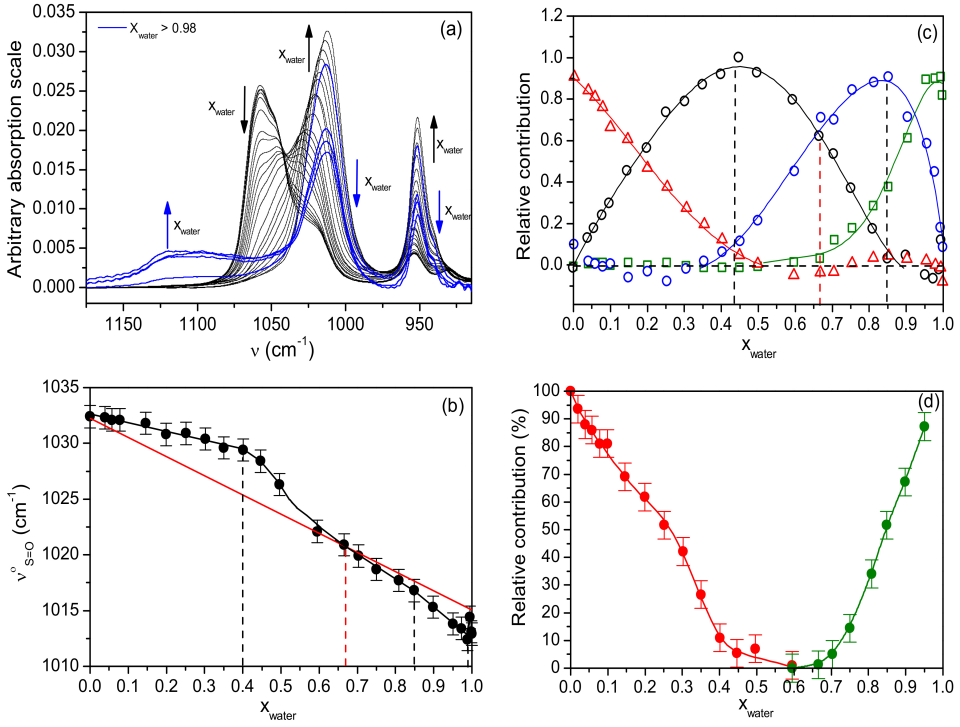

Figure 5: (a) FTIR spectra of DMSO–water mixtures in the range of the ν(S=O) and the rocking vibrations of the methyl groups depending on the solution composition. Blue lines represent the spectra for high water content in the mixtures ($x_w > 0.98$). Increasing/decreasing water mole fraction is shown by arrows. (b) The dependence of the ν(S=O) band position in maximum for DMSO forming hydrogen bonds with water (based on the spectra shown in Fig. S1 in the Supplementary Material) on the mole fraction of water in DMSO–water solutions. In the set of these residual spectra for $x_w > 0.1$, both low-wavenumber component bands determine the maximum of the complex band of ν(S=O). For $x_w < 0.1$ the band position of the low-wavenumber component has been taken into account. Solid red line indicates hypothetical ideal solutions. Vertical dashed lines indicate the composition of complexes: red line denotes the eutectic composition [33], while the black lines correspond to the observed complexes at their maximum concentrations. (c) Relative contributions of different forms of DMSO as a function of water mole fraction from the factor analysis of DMSO–water spectra: DMSO non-bonded to water (red △); molecular complex $3DMSO{\cdot}2H_2O$ (black ○); molecular complex corresponding to the core type complex: $1DMSO{\cdot}nH_2O$, where $n = 4 \div 6$, see text (blue ○); DMSO involved in the creation of the water cage (green □). (d) Relative contribution of DMSO not forming hydrogen bonds with water (red •), and DMSO involved in the creation of the water cage (green •) as a function of the mole fraction of water in DMSO–water solutions, obtained from the difference spectra method.

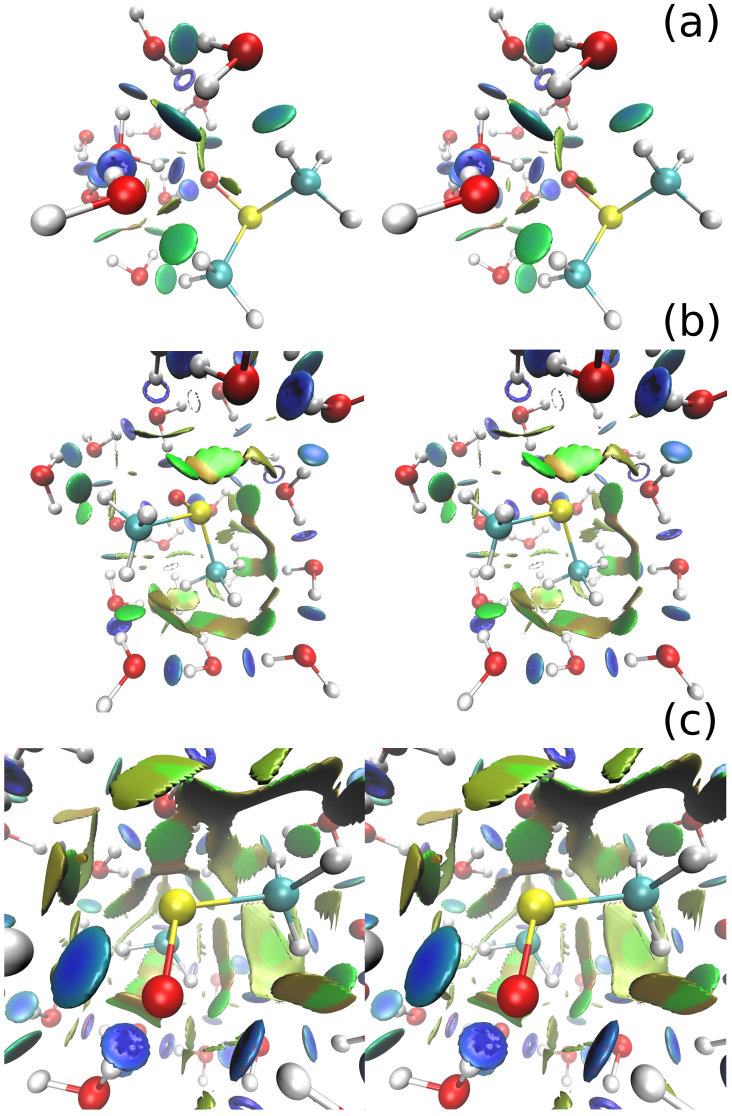

Figure 6: Stereo images of the results of weak interaction analysis by RDG function for larger DMSO–water complexes: a) 1DMSO·10H_2O, b) 1DMSO·20H_2O, c) 1DMSO·30H_2O. The meaning of various structures and colours is the same as in Figure 4. RDG calculated on the basis of electron densities obtained for ONIOM-optimized (B3LYP/aug-cc-pVQZ and B3LYP/cc-pVDZ) systems for high and low level calculation, respectively. See explanation in text.

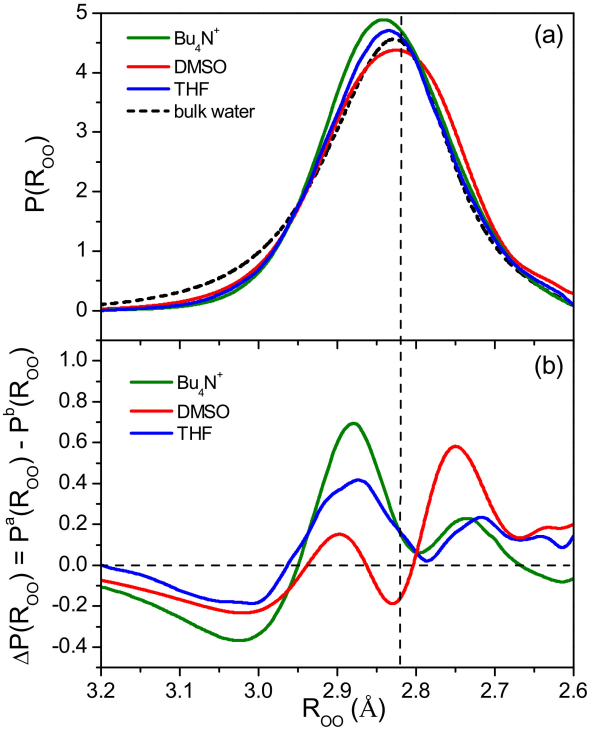

Figure 7: a) Interatomic oxygen–oxygen distance distribution function derived from the HDO spectra affected by DMSO, Bu_4N^+ [44], and THF [101], together with the bulk HDO distance distribution curve. (b) Differences between interatomic oxygen–oxygen distance distribution function for solute-affected water, $P^a(R_{OO})$, and the bulk water, $P^b(R_{OO})$, for DMSO, Bu_4N^+ [102], and THF. The vertical dashed line corresponds to the value of the most probable oxygen–oxygen distance in bulk water (2.83 Å).